Journal of Great Lakes Research 51 (2025) 102510

Contents lists available at ScienceDirect

Journal of Great Lakes Research

journal homepage: www.elsevier.com/locate/jglr

Development of a HAND-based flood risk assessment tool in Google Earth Engine for a data-scarce region in the US☆

Jobin Thomas[a], Subhami Mohan[a], Saumik Mallik[b], Thomas Oommen[a,*], Pengfei Xue[b,1], Guy Meadows[b,1], Navin Tony Thalakkottukara[a], Ryan Williams[b]

[a] Geology and Geological Engineering, University of Mississippi, Oxford, MS 38677, USA
[b] Great Lakes Research Center, Michigan Technological University, Houghton, MI 49931, USA

ARTICLE INFO

Communicated by Harvey Thorleifson, Ph.D.

Keywords:
Flood risk
HAND model
Great Lakes
Google Earth Engine
Flood resilience
Rural communities

ABSTRACT

Despite the decreased disaster resilience of rural communities in the Great Lakes region to flooding, flood mitigation efforts have been impeded by inadequate data and lack of appropriate tools for understanding flood risk. Development of such resources often requires data and computationally intensive approaches, which are challenging in data-scarce conditions. This study presents the development of a web application in Google Earth Engine (GEE) for flood risk assessment. The application utilizes the Height Above the Nearest Drainage (HAND) model and synthetic rating curve (SRC) for fluvial flood inundation modeling, the Simulating WAves Nearshore (SWAN) model for coastal flood inundation modeling, the United States Geological Survey (USGS) regional regression equations for estimating peak discharge, and depth-damage functions of the HAZUS-MH flood model for estimating losses due to building-level impacts. The GEE-based geospatial web application, which is operational across five counties in the Western Upper Peninsula (WUP) of Michigan, fulfills the requirement of the community and decision-makers to assess the risks caused by flooding in the region. We demonstrated the applicability of the tool in the Ontonagon River, Michigan, and the results indicate the suitability of the platform for implementing decisions, long-term planning, and understanding flood risk with a reasonable degree of accuracy.

1. Introduction

Extreme rainfall events (EREs) and subsequent floods have devastating consequences on society due to their significant disaster potential, human casualties, environmental impacts, and economic losses. Approximately one-fifth of the global population is directly exposed to 1-in-100-year floods, with nearly 70 % of the global exposure in South and East Asian countries, where infrastructure systems, including drainage and flood protection, are generally less developed (McDermott, 2022; Rentschler et al., 2022). Over the past three decades, flood events have resulted in cumulative global economic losses exceeding US$ 1.2 trillion, with US$ 300 billion incurred in the past 5 years alone (Swiss Re, 2023). In the United States, floods represent one of the most expensive natural disasters, in terms of both fatalities and economic losses (Cigler, 2017). Recent trends indicate an increase in the frequency and magnitude of floods driven by convective storms (Huang et al., 2022). Roughly 13 % of the population in the contiguous United States resides within the 1 % annual exceedance probability floodplain (Wing et al., 2018). According to the list of billion-dollar weather and climate disaster events, 11.7 % of the 377 billion-dollar events in the United States between 1980 and 2024 (March 8) were flood episodes attributable to EREs (Smith, 2024). Projected intensification of the hydrological cycle and rising sea levels in a much warmer (future) climate are expected to exacerbate the existing substantial flood hazard in many parts of the world, including the United States (Swain et al., 2020; Wasko et al., 2021). Other factors, such as population growth, rapid urbanization, socio-economic changes, and development in floodplains significantly drive up the flood risk by increasing flood exposure and vulnerability (Blum et al., 2020; Di Baldassarre et al., 2013; Früh-Müller et al., 2015; Han et al., 2020; Hu et al., 2018; Mazzoleni et al., 2021;

☆ This article is part of the special section entitled: 'Coastal Processes' published in Journal of Great Lakes Research.

* Corresponding author.
E-mail address: toommen@olemiss.edu (T. Oommen).

[1] *Given their roles as Guest Editors, Pengfei Xue and Guy Meadows had no involvement in the peer-review of this article and had no access to information regarding its peer-review. Full responsibility for the editorial process for this article was delegated to Harvey Thorleifson, Ph.D.*

https://doi.org/10.1016/j.jglr.2025.102510
Received 1 July 2024; Accepted 19 November 2024
Available online 6 February 2025

Winsemius et al., 2016). A recent study by Rentschler et al. (2023) highlighted that the expansion of human settlements in the most hazardous flood zones has notably surpassed the growth in non-exposed areas.

Coastal and fluvial flooding presents a formidable challenge to the communities across the Great Lakes region in the United States, particularly watersheds draining to Lake Superior (FEMA, 2023). The coastal communities have already witnessed a drastic rise in water levels in the Great Lakes, reaching record highs between 2019 and 2020 compared to the water levels over the previous century (Gronewold et al., 2021; Gronewold and Rood, 2019; Steinschneider, 2021). Projections suggest that these levels will continue to rise further with warming trends in the near future (Kayastha et al., 2022). While wind-driven storm surges and seiches in the Great Lakes, often linked to extratropical cyclones, drive water and waves onshore, inundating adjacent lowlands and coastal areas, EREs and associated runoff lead to inland (fluvial) flooding. The region has recently witnessed unprecedented occurrences of EREs and storms leading to flooding with massive economic losses. For instance, the Western Upper Peninsula (WUP) of Michigan recorded a 1000-year storm event on 17 June 2018, with 76.2 to 177.8 mm of rainfall in less than 6 h resulting in flash flooding and inundation. This event, known as the Father's Day flood, caused severe damage to infrastructure worth more than US$ 100 million (NWS, 2018; WUPPDR, 2020). Historically, the Great Lakes region has been a hub for mining industries, particularly along the shores. The risk of flooding introduces additional threats, including the potential contamination of drinking water sources with hazardous mining residues. The Federal Emergency Management Agency (FEMA) flood map, a product of the National Flood Insurance Program, serves as the major source of flood risk information in the United States. Nevertheless, roughly 75 % of FEMA flood maps are older than 5 years, and 11 % date back to the 1970s and 1980s. Many counties in the United States, including those in the WUP, remain unmapped (First Street Foundation, 2019), tending to underestimate the risk associated with high-magnitude floods. These conditions have instilled uncertainty in understanding the flood risk and highlight the necessity for developing tools to assess and visualize flood risk across the region. Recognizing the significant impacts of floods on rural communities and infrastructure, flood risk assessment is a prerequisite for communicating situational awareness, devising response plans, implementing targeted mitigation measures in development planning, allocating adequate resources, making informed decisions, and enhancing disaster resilience, thereby building sustainable, climate-resilient communities across the Great Lakes region.

Implementing efficient risk reduction measures requires reliable estimates of the areal extent and depth of inundation for flood events. State-of-the-art flood risk models typically incorporate a model chain that includes either hydrological models or frequency analysis for estimating flood discharge magnitude, hydrodynamic models for mapping flood inundation, and damage (vulnerability) functions for risk assessment (Grigg, 2023). In the United States, the HAZUS-MH-based flood risk analysis is the most prevalent approach for quantifying flood risks and facilitating informed decision-making (Schneider and Schauer, 2006). The flood risk assessment in the HAZUS-MH flood model involves flood hazard analysis and flood loss estimation, where the former delineates the inundation extent and depth for riverine and coastal flooding, and the latter computes economic losses using the depth-damage functions (Scawthorn et al., 2006a, 2006b). Generally, three major approaches have been used for riverine flood inundation mapping: empirical methods, hydrodynamic models, and simplified conceptual models (Teng et al., 2017). While empirical approaches use observed data, hydrodynamic models simulate inundation primarily by solving one-dimensional Saint-Venant equations or two-dimensional shallow water equations. Although two-dimensional hydrodynamic models have been extensively used in flood inundation mapping and hazard assessment frameworks, their high computational and data requirements restrict their application at large spatial scales or in data-scarce conditions, such as watersheds draining the Great Lakes region. As an alternative, researchers have developed simplified models, such as the Height Above the Nearest Drainage (HAND) and AutoRoute for approximate inundation mapping with minimal input data and computational resources (Follum, 2013; Nobre et al., 2011). The use of these low-complexity models mitigates some of the limitations of hydrodynamic models while providing a preliminary estimation of flood-prone areas. For example, the HAND model only requires the digital elevation model (DEM), which is available over large geographic scales and performs first-order approximations of fluvial flooding (Afshari et al., 2018; Johnson et al., 2019; Thalakkottukara et al., 2024).

The HAND represents a terrain derivative that indicates the difference in elevation between a given point (pixel) in a DEM and the nearest stream channel to which the point drains, following the local drainage direction (Rennó et al., 2008). The HAND value of any given pixel implies the water level required for inundation, and hence, the inundation depth corresponding to a given flood stage can be estimated as the difference between the water level and the HAND value. Various approaches based on the HAND model have been demonstrated for flood inundation mapping. For instance, Zheng et al. (2018a) developed an approach utilizing a synthetic rating curve (SRC), which relies on the relationship between reach-averaged channel hydraulic parameters and stage height, using HAND and other DEM-based hydrological derivatives. The SRC assumes a one-dimensional steady-state flow condition with normal depth. Recently, Unnithan et al. (2024) proposed another conceptual flood inundation model for data-scarce environments, integrating the HAND model and Manning's equation, and utilizing the empirically derived global river geometry data (Andreadis et al., 2013). Although the HAZUS-MH flood model also solves Manning's equation for computing flood elevations, the methods adopted among these approaches (i.e., FEMA, 2009; Unnithan et al., 2024; Zheng et al., 2018a) differ. Unnithan et al. (2024) utilized the dynamic Budyko hydrological model to generate runoff rasters. This approach used empirical bankfull-width and -depth values extracted from a global river channel database (Andreadis et al., 2013) and solved for the flow velocity using Manning's equation, assuming a rectangular channel geometry. An exponential distribution curve was fitted to the elevation and distance of each pixel of the channel reach to the downstream mouth to estimate the conceptual slope, with a uniform roughness coefficient of 0.03. The pre-processed HAND inundation extent and corresponding flood depth were subsequently mapped to the conceptually derived discharge values. Zheng et al. (2018a) introduced a method to derive reach-averaged channel geometry properties, such as cross-sectional area, and hydraulic radius, for a uniform reach-average water level using the HAND. These channel hydraulic properties, along with channel bed slope and Manning's n, were used to predict the discharge corresponding to the water depth at uniform flow. By computing the discharge for various water depths, a SRC was generated, which can be used to generate flood inundation corresponding to any given (observed/simulated) discharge. In the HAZUS-MH flood model, flood elevations are computed using Manning's equation with cross-section geometry, roughness coefficient (default value of 0.08), and friction slope as inputs. For Level 1 analysis, regional regression equations developed by the United States Geological Survey (USGS) are used to predict discharge for a specific return period. Given the discharge value, Manning's n, and friction slope, Manning's equation iteratively solves for the flood depth (FEMA, 2009). In another study, Jafarzadegan et al. (2022) developed a composite hydrogeomorphic index, which is the product of HAND and distance to the nearest drainage, and hydrogeomorphic threshold operative curves for rapid real-time flood hazard assessment in coastal areas.

Being a low-complexity model with computational efficiency compared to hydrodynamic models, HAND-based approaches have been improved and validated across diverse fluvial environments and a broad range of spatial scales for rapid flood simulation and forecasting (Aristizabal et al., 2023; Fang et al., 2023; Jafarzadegan and Merwade, 2019; Johnson et al., 2019; Richardson and Beighley, 2024; Zheng et al., 2018b), resulting in the development of real-time, web-based flood inundation mapping applications. For example, Hu and Demir (2021) developed a standalone client-side web system for estimating the extent of flood inundation for flood-prone regions in Iowa. In this approach, three parameters (HAND threshold, drainage threshold, and absolute height) were incorporated to address the challenges during the web-based implementation of the HAND model and were adjusted to approximately map the flood inundation. Subsequently, Li and Demir (2022) developed a client-side, web-based, real-time, and interactive inundation mapping system that can be implemented in any region with customized data processing and analysis options at the end-user level. In a separate effort, Liu et al. (2018) developed a cyberGIS framework for continental flood inundation mapping, which couples HAND with National Oceanic and Atmospheric Administration (NOAA) National Water Model forecasts, facilitating near real-time inundation prediction for the conterminous United States. The streamflow forecasts from the National Water Model are translated to water depth using the hydraulic properties and SRC derived from HAND (after Zheng et al., 2018a). Chaudhuri et al. (2021) presented a similar flood inundation modeling framework, InundatEd, using HAND and Manning's equation, which is implemented in a big-data discrete global grid system-based architecture with a webGIS platform for selected regions in Canada lacking flood risk maps. The InundatEd framework uses flood frequency analysis and regional regression for discharge estimation, the HAND-based solution of Manning's equation for flood inundation modeling, and the depth-damage functions of the HAZUS for estimating the losses. Scriven et al. (2021) developed a customized tool in ArcGIS Pro, viz., CERC-HAND-D, to create acceptable flood maps using HAND and SRC, which has the potential to develop a web-based flood mapping application.

In this study, we aim to develop a simple and user-friendly flood risk assessment tool (one of the tools in the Rural Hazard Resilience Tools, RHRT) for rural communities in the WUP (Michigan) of the Great Lakes region. The tool is designed for approximate mapping of flood inundation and associated economic losses due to building-level impacts. The flood risk assessment tool is a web application based on Google Earth Engine (GEE), leveraging the availability of high-resolution Light Detection and Ranging (LIDAR)-derived DEM data and building characteristics of the region for estimating the flood risk. The GEE has been widely used for flood inundation mapping and monitoring, largely utilizing publicly available satellite image collections (e.g., Li and Demir, 2024; Tripathy and Malladi, 2022; Wu et al., 2019). However, our approach integrates the HAND model and SRC for fluvial flood inundation mapping (Zheng et al., 2018a), the USGS regional regression models for flood frequency statistics (Jennings et al., 1994), the Simulating WAves Nearshore (SWAN) model for coastal flood inundation mapping, and the depth-damage functions in the HAZUS Flood Assessment Structure Tool for loss estimation (FEMA, 2009). We harnessed the cloud computing infrastructure of GEE and customized ArcGIS Pro and Python tools for implementing the web-based flood risk assessment application. This approach facilitates a comprehensive and efficient assessment of flood risk, contributing to the resilience and adaptation of rural communities in the Great Lakes region.

2. Study region

This study focuses on the development of a flood risk assessment tool for rural communities and various stakeholders in five counties in the WUP region of Michigan. These counties, viz., Houghton, Baraga, Keweenaw, Ontonagon, and Gogebic, are bordered by Lake Superior (Fig. 1). The study region covers a land area of roughly 4800 mi^2 (approx. 12,430 km^2) and has a total population of 68,211. The topography of the WUP ranges from rugged, near mountainous areas to broad-level plains and flat topography, interspersed with numerous swamps and lakes (mostly located in glacial moraines and outwash). The land surface elevation varies from about 600 feet (182.9 m) above the North American Vertical Datum of 1988 along the Lake Superior shoreline to 1979 feet (603.2 m) in Baraga County. The WUP has a unique and complicated geological history, marked by multiple tectonic episodes, resulting in an exceedingly diverse array of lithological formations, predominantly of Precambrian ages, with significant concentrations of metallic minerals including copper and iron (Bornhorst and Barron, 2011). The region is drained by numerous rivers flowing towards Lake Superior. Some of the major rivers in the region include Ontonagon, Sturgeon, Presque Isle, Black, and Montreal. The region experiences a humid continental climate with a warm summer (Köppen-Geiger climate

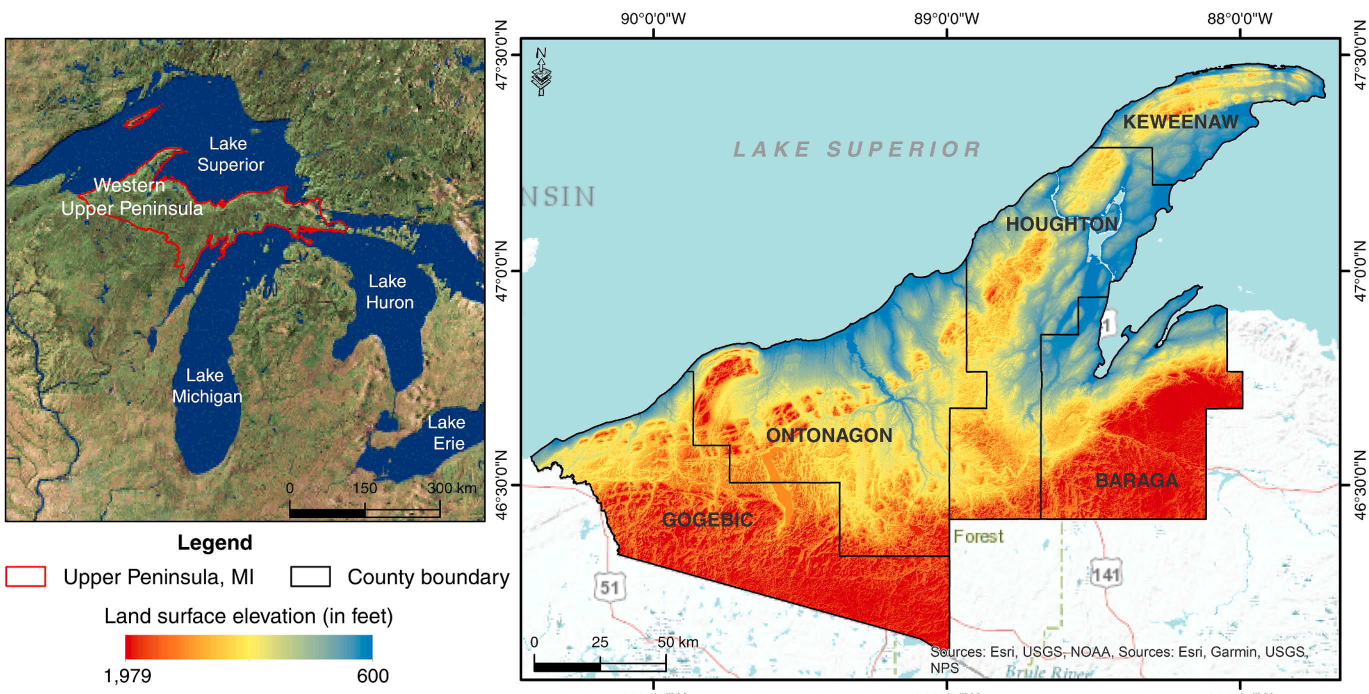

Fig. 1. Map showing the counties in the WUP region, Michigan.

class: Dfb), which is significantly influenced by Lake Superior. Based on the climate data between 1981 and 2010, the mean annual temperature of the region was 40.6°F (4.8 °C), and the mean annual precipitation was 32.0 in. (813 mm) (MRCC, 2012). The land use/land cover of the study region is predominantly forested (70 %) and wetlands (20 %). Agricultural land use and cultivated areas cover about 3 % and developed urban areas cover roughly 4 % of the land area (Dewitz, 2023). The soils of the region are primarily developed from glacial-related sediments. Spodosols cover the majority of the WUP, followed by Alfisols, and the soils are characterized by the dominance of clayey or sandy fractions. Spodosols, primarily composed of sandy parent materials, are typically subject to intense leaching, resulting in low fertility and limited water storage capacity.

3. Methodological framework

The overall methodology adopted in this study is illustrated in Fig. 2. The development of the flood risk assessment tool involves three phases: (1) flood inundation modeling, (2) flood damage assessment, and (3) designing the web application in GEE. The flood inundation modeling compartment integrates the HAND model, SRC, USGS regional regression models, and SWAN model to simulate flood inundation characteristics, whereas the flood loss assessment utilizes the depth-damage functions in the HAZUS-MH flood model to estimate the potential economic losses due to building-level impacts from flooding. The third phase involves the development of a user-friendly web application in GEE. This application allows users to interact with the flood risk assessment tool and visualize the results. The subsequent sections provide a detailed description of the methods.

3.1. HAND model

The HAND model requires a hydrologically corrected DEM as input data. In this study, we used high-resolution topographic elevation data (i.e., LIDAR DEM), which was resampled to a spatial resolution of 9 feet x 9 feet (~3 m x 3 m). Artificial barriers in the DEM, largely due to roads, were removed by enforcing the USGS National Hydrography Datasets (i.e., NHDPlus high-resolution streams) into the resampled DEM. The hydrologically conditioned DEM was generated from the stream-burned DEM using the digital terrain conditioning workflow developed by

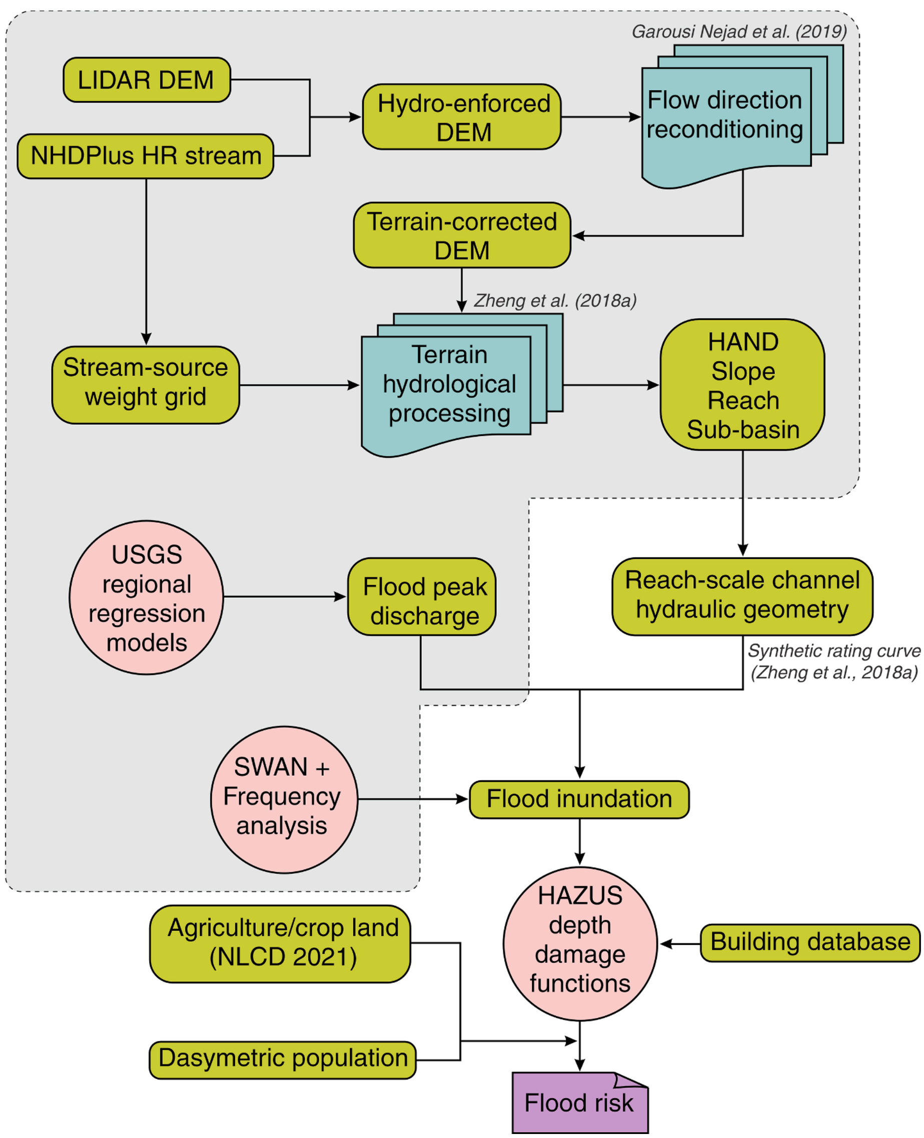

Fig. 2. Methodological framework adopted for the flood risk assessment tool in GEE. Terrain hydrological processing includes standard workflow for generating flow direction, flow accumulation, and stream rasters. The processes within the shaded portion were executed mostly using customized tools in ArcGIS Pro and Python, rather than in GEE.

Garousi-Nejad et al. (2019). Despite using the channel initiation threshold for delineating the drainage network from the DEM, we utilized the NHDPlus streams to identify the upstream channel head of each first-order stream, which was used as the stream source (headwater) weight grid. We noted some inconsistencies in the NHDPlus streams for the WUP region, which were rectified using the USGS topographic maps (1:24,000 scale) available as base maps in ArcGIS Pro. Flow direction rasters were derived from the hydrologically conditioned DEM using the D8 function for stream network delineation and the D∞ function for HAND generation. The stream source weight grid was used to derive the weighted flow accumulation raster, which was then used to define the stream raster. Finally, the HAND was computed from the stream raster and the hydrologically conditioned DEM using the D∞ flow distance function. The stream and flow direction (D8) rasters were further utilized to generate the stream reaches and sub-basins. In this study, we used the TauDEM (standalone) toolbox for the hydrological conditing of the DEM and spatial analyst tools (in ArcGIS Pro) for preprocessing, hydrological terrain analysis, and generating the HAND raster. A detailed description of the methods to compute the HAND raster using the NHDPlus streams is provided by Zheng et al. (2018a).

3.2. Generation of SRC

In this study, we followed the conceptual framework of Zheng et al. (2018a) for deriving reach-averaged channel hydraulic geometry and SRC for flood inundation mapping. For a given sub-basin, the input data required to generate SRC includes HAND and slope rasters, as well as reach characteristics. First, we delineated the reaches and sub-basins of the WUP region from the DEM using hydrological terrain analysis (in Section 3.1). Subsequently, the HAND and slope rasters were extracted for each sub-basin. For any given pixel *i*, the HAND raster implies the difference in elevation of the pixel *i* and the downslope pixel *j* where the flow from the pixel *i* enters the nearest stream channel, following the local drainage direction. Therefore, the inundation depth in a pixel for any flood stage can be calculated as the difference between the stage height and the HAND value. The inundation area and average inundation depth of each sub-basin were estimated for varying stage heights up to 25 feet (7.62 m) using the HAND raster of the sub-basin. We computed length (L) and average bed slope (S) of the reach from the DEM-derived stream network. For a given stage height, we derived the cross-sectional area (A), wetted perimeter (P), and hydraulic radius (R) of the reach. Although the surface roughness varies along the reach, we assumed a constant value (0.05) for Manning's n in this study. We computed the discharge (Q) for different stage heights using Manning's equation (Eq. (1), resulting in the generation of SRC:

$$Q_i = \frac{1.49}{n} \times A \times R^{\frac{2}{3}} \times S^{\frac{1}{2}} \tag{1}$$

where Q_i is the predicted discharge (in cubic feet/second) for the stage height, i. The SRC relates the stage height to Q, which is assumed to be uniform along the reach. This SRC can be used for converting the modeled flood discharges into corresponding flood inundation depths.

3.3. Estimation of peak flood discharge magnitudes

In ungauged watersheds, such as those draining much of the WUP region, estimating flood discharge magnitude presents a major challenge. Given the limited availability of river gauge data in the watersheds of the area, we utilized the regional regression equations developed by the USGS to compute flood discharge magnitudes for specific return periods. The USGS developed regional regression equations to estimate peak-flow frequency statistics for ungauged watersheds across all states of the United States. These equations statistically correlate streamflow with different watershed and climatic characteristics as explanatory variables for gauged sites and are used to transfer flood characteristics from gauged to ungauged sites using these predictor variables (Jennings et al., 1994; Ries et al., 2024). The regression equations developed for Michigan streams predict peak discharges for recurrence intervals ranging from 5 to 100 years. The explanatory watershed variables of the regression equations are contributing drainage area (in square miles), main-channel slope (in feet/mile), percentage length of mainstream channel passing through swamps, lakes, or ponds, slenderness ratio, which is defined as the ratio between the square of channel length and the contributing drainage area, and 100-year 24-hour rainfall (in inches). In addition, the equations also include seven surficial geologic material characteristics (as a percentage of the contributing drainage area) and a regional factor. The surficial geologic variables are (1) lacustrine clay and silt, (2) coarse-textured glacial till, (3) end moraines of fine-textured till, (4) medium-textured glacial till and end moraines of medium-textured glacial till, (5) peat and muck, (6) postglacial alluvium, glacial outwash sand and gravel and postglacial alluvium, and ice-contact outwash sand and gravel, and (7) thin to discontinuous glacial till over bedrock (Jennings et al., 1994).

We developed customized tools in ArcGIS Pro for estimating the watershed variables using the DEM, DEM-derived channel reaches and sub-basins data. We utilized the National Wetland Inventory open data maintained by the Michigan Department of Environment, Great Lakes, and Energy (EGLE) for identifying the stream channel sections passing through swamps, lakes, or ponds (EGLE, 2020). The 100-year 24-hour rainfall was computed from the spatially interpolated, high-resolution NOAA Atlas 14 precipitation frequency estimates (NOAA, 2022). The surface geological characteristics were extracted from the Quaternary Geology of Northern Michigan (1:500,000 scale) (Farrand and Bell, 1982). Michigan is divided into five hydrologic regions, and for this study, we used the regional factor for the Upper Peninsula (i.e., Region 1). While the flood risk assessment tool aims to provide flood inundation characteristics for 25-, 50-, 100- and 500-year return periods, the regression equations provide peak discharges only up to a recurrence interval of 100 years. Hence, we extrapolated the 5- to 100-year flood discharges predicted by the regression models to 500-year flood discharge assuming a log-linear relationship.

3.4. Flood inundation mapping

Given the flood discharge magnitudes for any reach from the USGS regional regression models, the corresponding flood inundation depths can be generated from the SRC. Thus, the flood inundation depths for 25-, 50-, 100- and 500-year return periods were estimated for each sub-basin, which serves as the fluvial (inland) flooding layers. Although the HAND model provides an approximation of inundation due to fluvial flooding, it tends to have limited capability to represent the inundation due to coastal flooding along the lake shore (Gutenson et al., 2023). Hence, we used the SWAN model for simulating nearshore wave climate extremes, also for 25-, 50-, 100-, and 500-year return periods, and their impacts on episodic water levels in Lake Superior. Lake water level data from four NOAA gauge stations along the southern shore of Lake Superior (i.e., Duluth, Ontonagon, Marquette, and Port Iroquois) was utilized to compile a comprehensive temporal dataset that includes both baseline water levels and temporary surges caused by storms, high winds, atmospheric pressure changes, and other meteorological conditions. The annual maximum water levels from these stations were extracted and fitted to generalized extreme value and Gumbel distributions using maximum likelihood estimation. The goodness of fit was assessed using Kolmogorov-Smirnov, Anderson-Darling, and Cramer-von Mises tests, along with Akaike Information Criterion and Bayesian Information Criterion, leading to the selection of the Gumbel distribution as the preferred model for annual maximum static water level with surge. Return levels for 25-, 50-, 100-, and 500-years were computed by inverting the cumulative distribution function of the fitted distributions at corresponding probabilities. These return levels were linearly extrapolated along the longitudinal axis to extend values to each SWAN wave model node within the study area, providing a comprehensive view of static water return levels, storm surge, and extreme wave setup and runup across the southern shores of Lake Superior.

To address the underestimation of extreme wave events by the SWAN model (Dreier et al., 2020; Huang et al., 2021), a multi-step amplification process was implemented and verified against observed wave heights from seven separate US Army Corps of Engineers (USACE) Wave Information Study (WIS) stations, refining the predictions for wave heights. The annual maximum significant wave heights were extracted and fitted to the Gumbel distribution using maximum likelihood estimation, similar to the approach used for water levels. Empirical formulations by Mase (1989) were applied to estimate wave runup, accounting for changes in wave heights over return periods of 25-, 50-, 100-, and 500-years. By integrating the wave runup component with the corresponding water level of similar return period, the wave-induced total water levels were calculated across the entire study area. We used a simple mapping approach to translate the predicted water levels for different return periods (i.e., 25-, 50-, 100-, and 500-year) to coastal flood inundation depths. We used the spatially varying lake water levels and the DEM and estimated the inundation depths by performing a conditional statement (in ArcGIS Pro) for subtracting the DEM from the water level wherever the DEM is less than the water level.

3.5. Flood damage assessment

The damage to buildings due to flood inundation was assessed based on the flooding depth, using a depth-damage curve specific to each type of occupancy. We used the depth damage (vulnerability) function library in the HAZUS Flood Assessment Structure Tool, which is a collection of readily-available depth-damage curves, compiled from a variety of sources (e.g., Federal Insurance and Mitigation Administration, USACE, and the USACE Institute for Water Resources) to calculate building-level flood impacts with user-provided flood depth and building data (FEMA, 2009, 2011). The flood inundation depths estimated using the fluvial and coastal flood inundation models were provided as the flood depth grid. The building level data were collected from the tax assessor office and equalization department of the five counties in the WUP region. Based on various building attributes, such as occupancy type, replacement cost (in US $), area (in square feet), number of stories, foundation type, first-floor elevation or height above grade of finished first floor (in feet), depth damage functions were assigned to buildings. Flood depth was then extracted at every building and used as a depth damage function parameter to calculate flood losses (in US $). Flood-generated debris was estimated using the building area. The coastal and inland flooding scenarios use different depth damage functions for loss estimations. If a building is affected by both coastal and inland flooding, the depth damage function will be selected using the larger magnitude of the inundation depth.

3.6. Application programming interface in GEE

The web-based application of the flood risk assessment tool, to estimate the flood inundation extent and depth, and potential impacts of floods on building infrastructure, was developed in GEE. The GEE leverages Google's cloud platform for planetary-scale analysis of Earth Science data, assists in developing full-featured JavaScript, Python, and REST APIs, and makes it simple to publish apps. With these capabilities, the platform ensures access to various end-users with ease of use. We used the JavaScript API in the web application development on the GEE platform. The major input datasets used for the flood inundation mapping in the web-based application include the HAND raster, sub-basin, and reach shapefiles, and the USGS regression based flood discharge magnitudes for varying return periods (25-, 50-, 100- and 500-year) (Fig. 2). A User-Defined Facility (UDF) database with the required building attributes in the precise formats specified in the technical manual of the HAZUS Flood Assessment Structure Tool serves as the user-defined input for flood loss estimation. We uploaded the HAZUS lookup tables for flood loss assessment to the platform, which is significant in executing the depth damage function to calculate the damage losses. We also used the gridded dasymetric population data (USEPA, 2020) and National Land Cover Database 2021 (Dewitz, 2023) for quantitative estimation of the affected population and agricultural areas during the flood events. The web-based application provides an interface to select the area of interest (AOI) and the flood return period (Fig. 3). The code internally executes the application after the selection of AOI and flood return period to generate the results on a panel widget in the map viewer. The detailed methodology of the estimation of building losses is available in FEMA (2009) and Scawthorn et al. (2006b).

4. Results and discussion

The GEE-based flood risk assessment tool was developed to estimate flood inundation characteristics, affected population and agriculture areas, and economic losses due to building-level impacts for flood events of 25-, 50-, 100-, and 500-year return periods. This hazard communication engine serves as a platform for the rural communities in five counties of the WUP to map the probable areas under flooding, estimate potential assets and facilities at risk, and calculate possible losses from catastrophic flood events in the area. The primary outputs generated by the tool consist of a flood hazard map, building exposure data, and damage estimates. Flood hazard maps for specific return periods provide an overview of areas that are prone to flooding based on topography and the probable depth of flood inundation in different parts of the affected area. Building exposure data includes information about the location, type, and characteristics of buildings in the affected area, whereas damage estimates cover the number of affected buildings, economic losses, and debris volume. The tool also provides estimates of the number of the affected population, and the extent of agricultural areas in the region.

As a testing domain for demonstrating the tool, we generated potential flood inundation zones for a 100-year return period event in the downstream reach of the Ontonagon River and nearby areas in Ontonagon County, Michigan. Fig. 4 shows the inundation extent and economic losses for a 100-year return period flood. The flood inundation extent includes both inland and coastal flooding. The analysis shows that roughly 1836 ha of area, including 105 ha of cropland, are predicted to be under inundation for a 100-year flood event. The widget panel also provides information about the number of exposed individuals and buildings, as well as the expected economic losses.

While the GEE-based flood risk assessment tool offers quantitative estimates of flood inundation and associated risk for flood events with varying return periods, significant challenges arise from uncertainties within the model chain. In this approach, potential sources of uncertainty could be associated with the SWAN model, HAND-based SRC, estimation of peak flood discharges, and depth-damage functions. Various researchers (e.g., Afshari et al., 2018; Thalakkottukara et al., 2024) have noted that the performance of HAND-model is sensitive to topographic conditions and valley settings, primarily due to the simplified representation of channel flow hydraulics. The derivation of reach-averaged channel hydraulic properties in the HAND-based SRC assumes uniform flow and uses Manning's equation over non-homogeneous stream reaches. Typically, the uncertainty in the HAND-SRC approach is largely contributed by Manning's n and hydraulic geometry (Diehl et al., 2021; Godbout et al., 2019; Johnson et al., 2019; Zheng et al., 2018a). In this approach, we used a uniform Manning's n of 0.05, and the selection of Manning's n values is a major source of uncertainty (Zheng et al., 2018a). However, incorporating more reliable estimates of variable roughness (Manning's n) could significantly improve the performance of SRC (Godbout et al., 2019). Another limitation is the exclusion of hydraulic structures (e.g., culverts, bridges) from the model. In such cases, Manning's equation may be insufficient to

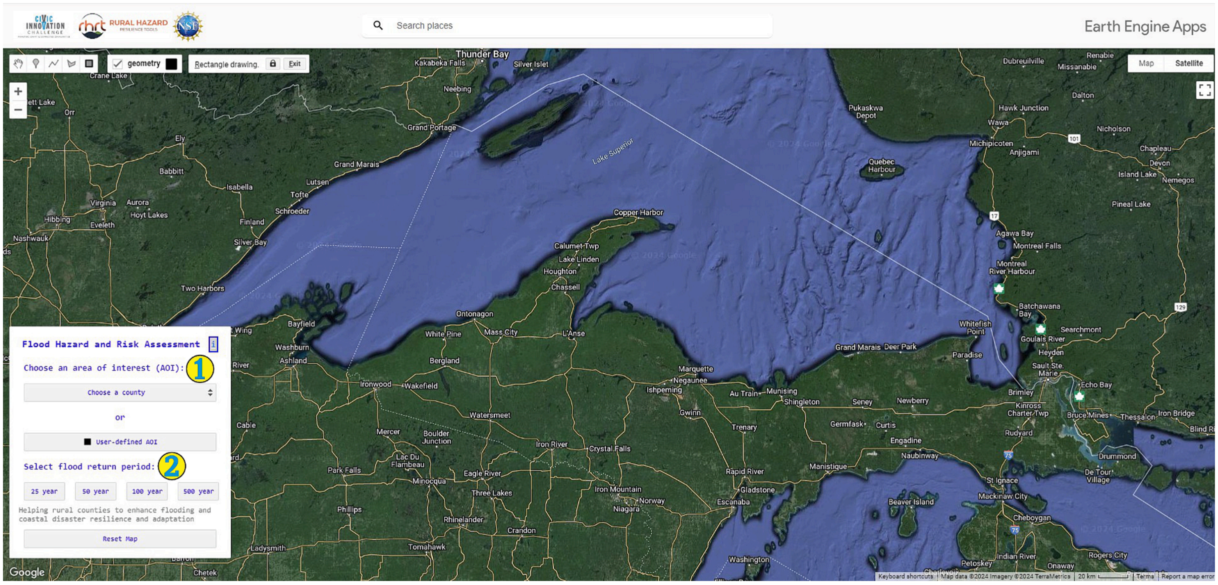

Fig. 3. Graphic user interface of the GEE-based flood risk assessment tool in RHRT. The panel widget has (1) provisions given to run the model for an entire county or a given AOI and (2) options to select the flood recurrence interval (25-, 50-, 100- and 500-year) for the end-user.

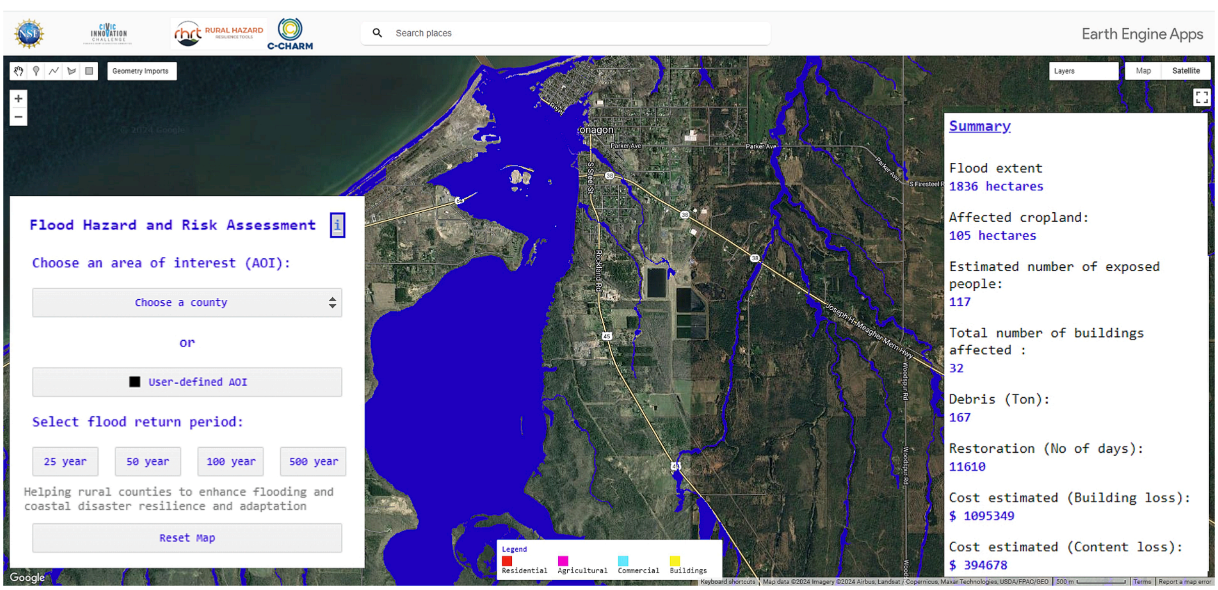

Fig. 4. Results of the flood risk evaluation in Ontonagon River and adjacent areas (Ontonagon County, Michigan).

accurately relate river discharge to stage height. Further, roads, bridges, and other hydraulic structures, such as culverts and dams can negatively impact the accuracy of SRC (Godbout et al., 2019). Although we simultaneously considered the fluvial and coastal flooding, we did not model their interactions and boundary effects, which could add uncertainty in estuarine conditions. Another major source of uncertainty is in the estimation of peak discharge, primarily due to the empirical nature and inherent assumptions of the models. We derived the model input data from a wide variety of sources with different spatial scales. The accuracy of streamflow estimates for Michigan streams using the equations depends on flow characteristics, where the extremes (i.e., peak flow and low flow) have the highest standard errors (Holtschlag and Croskey, 1984). However, this uncertainty can be partially addressed by computing the peak flow values with a desired level of confidence. In order to assess the performance of the USGS regional regression equations in predicting peak discharge, we compared the model-predicted discharges (for 10-, 100- and 500-year return periods) with the flow discharge database of EGLE (Fig. 5). While a general linear relationship was noted between predicted discharges and the discharge data of EGLE for various rivers, significant differences exist in rivers with low to moderate flood discharges, highlighting uncertainties in the hydrological model. Uncertainty in flood loss estimates is also heavily influenced by the data and methods used in the risk modeling process (Tate et al., 2015), where the building inventory and damage functions are important sources of epistemic uncertainty (Saint-Geours et al., 2015). Although we used a building database that was collected from the equalization departments and assessor's office of the respective counties in the WUP region, many of the data records were incomplete. In such cases, we filled the data gaps either statistically or using default values provided in the HAZUS-MH technical manual (FEMA, 2009).

We compared the flood inundation for a 100-year return period event simulated by the GEE-based flood risk assessment tool and the HEC-RAS 2D model in selected river segments within the WUP watersheds to assess the general agreement between these approaches (Fig. 6).

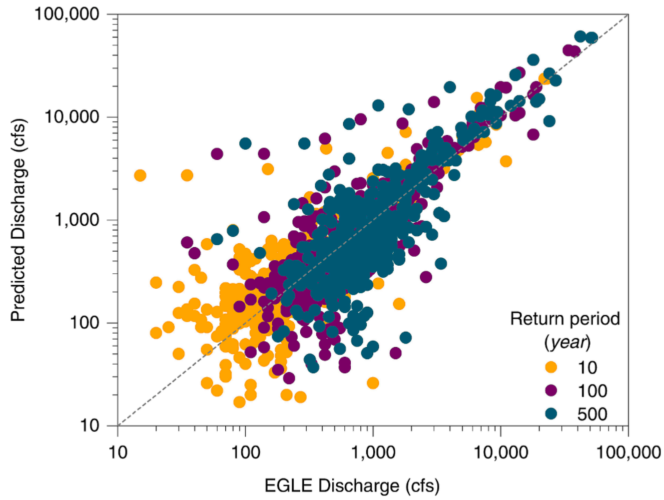

Fig. 5. Relationship between discharge predicted by the USGS regression models (in this study) and EGLE flood discharge.

The comparison of simulated flood inundation extent and depth reveals that the GEE-based tool provides results comparable to the HEC-RAS 2D model simulations. However, the integration of the USGS regional regression models and HAND-SRC approach underestimated the flood inundation extent and depth, notably in the river segments of smaller watersheds (e.g., Trap Rock River and Little Carp River). Underestimation of flood inundation characteristics in HAND-based approaches has been reported in various hydrological environments (e.g., Afshari et al., 2018; Johnson et al., 2019; Thalakkottukara et al., 2024).

The GEE-based flood risk assessment tool is one component of the RHRT (https://www.wuppdr.org/rhrt), which is a suite of tools to help rural communities in the WUP region enhance flooding and coastal disaster resilience and adaptation. In addition to the flood risk assessment tool, a web application for collecting crowdsourced data, including photographs of flood events, and a geospatial platform to visualize the flood risk, critical infrastructure, and community resilience are also functional. The crowdsourced data collection application is an example of citizen science engagement that allows the community members and public to upload flood inundation pictures (in case of an event) to address current data gaps for improved flood hazard modeling by validating the HAND-based flood model and improve the automated flood information extraction efforts using machine learning algorithms. The geospatial visualization platform is designed to disseminate flood risk information to rural communities and to help the decision-making authorities, emergency service professionals, and other community leaders make more informed decisions for flood risk mitigation. Since the methodological framework of the RHRT is cost-effective, less resource-intensive, and easy to implement, these tools are scalable and transferable. Although the scope of these tools is primarily flooding, these tools can be extended to other natural hazards too. Therefore, the development of the RHRT serves as a primary measure to transform the rural communities in the Great Lakes region into a disaster-resilient and risk-informed society.

5. Conclusion

The Great Lakes region in the United States is vulnerable to coastal and fluvial flooding, posing significant challenges to local communities. Despite the necessity of flood risk assessment for effective risk communication, development planning, and informed decision-making, the lack of suitable tools-owing to high data and computational

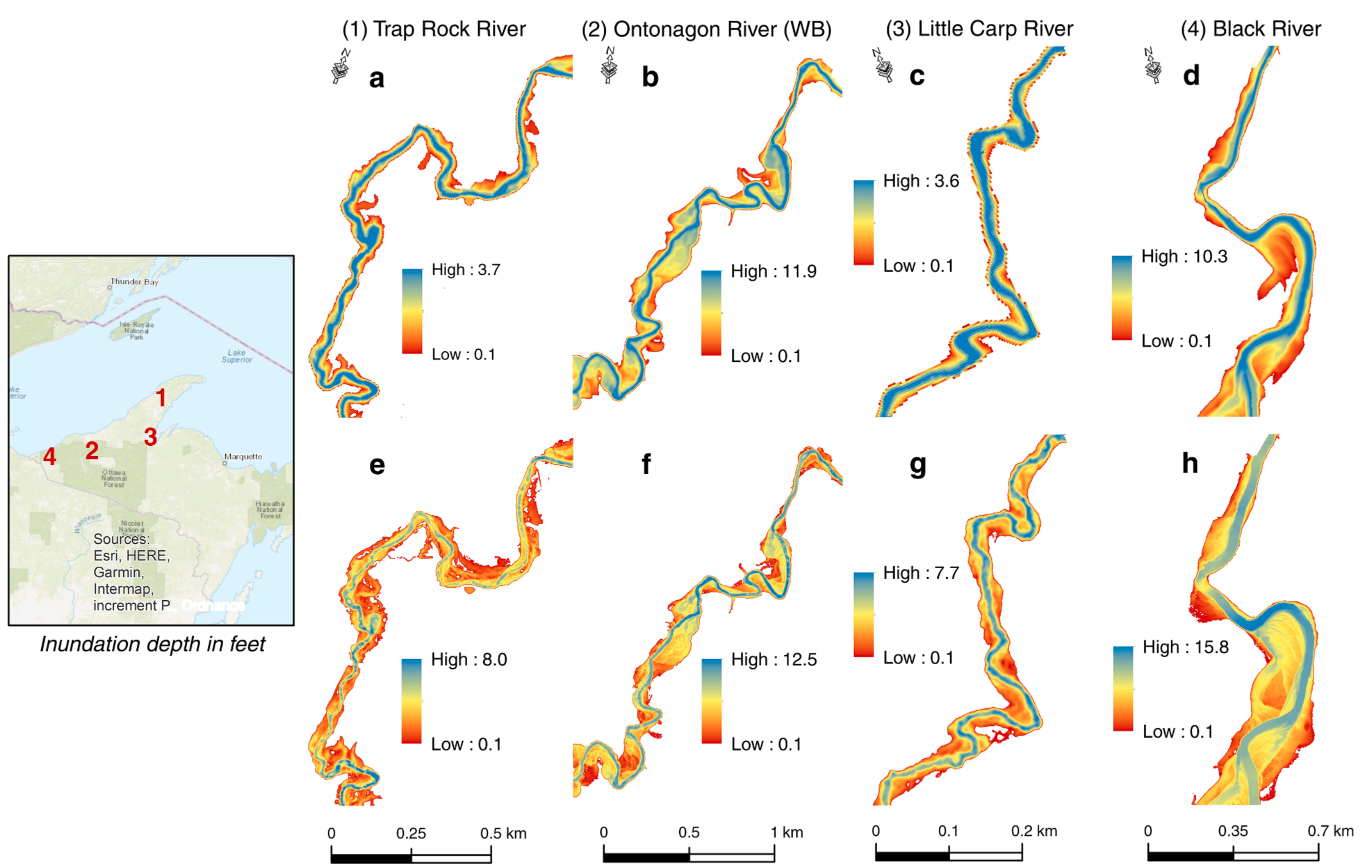

Fig. 6. Comparison of fluvial flood inundation extent and depth for a 100-year flood in different rivers of the region using the GEE-based (HAND-SRC) approach (a, b, c, d) and HEC RAS-2D (e, f, g, h).

demands-presents a major obstacle to enhance disaster resilience and adaptation in rural communities across the region. This study describes the development of a web application in Google Earth Engine (GEE) for flood risk assessment. This application is part of a consortium of open-source tools, viz., Rural Hazard Resilience Tools (RHRT), which also include a web application for collecting crowdsourced data and a geospatial platform for visualizing flood risk, critical infrastructure, and community resilience. The tool is operational in five counties in the WUP region of Michigan (Houghton, Baraga, Keweenaw, Ontonagon, and Gogebic), all of which border Lake Superior. While the tool integrates the Height Above the Nearest Drainage (HAND) model, synthetic rating curve (SRC), and USGS regional regression model to simulate fluvial flood inundation characteristics, the tool utilizes the Simulating WAves Nearshore (SWAN) model and frequency analysis for coastal flooding. The flood loss assessment uses the depth-damage functions in the HAZUS-MH flood model to estimate potential economic losses due to building-level impacts from flooding. We developed a user-friendly web application in GEE, enabling users to interact with the flood risk assessment tool and visualize the results. We generated potential flood inundation zones for a 100-year return period event in the downstream reach of the Ontonagon River and nearby areas in Ontonagon County, Michigan. This demonstration showcases the appropriateness of the tool in risk communication and assessment, thereby enhancing the resilience of rural communities to flood hazards.

6. Code availability

The codes used for the development of the flood risk assessment tool are available on GitHub at [https://github.com/CivicInnovation/HC-engine]. The repository includes all scripts and documentation necessary to reproduce the results presented in this paper.

CRediT authorship contribution statement

Jobin Thomas: Writing – review & editing, Writing – original draft, Visualization, Software, Resources, Methodology, Investigation, Formal analysis, Data curation, Conceptualization. **Subhami Mohan:** Writing – review & editing, Writing – original draft, Visualization, Software, Methodology, Formal analysis, Data curation. **Saumik Mallik:** Writing – original draft, Software, Resources, Methodology, Investigation, Formal analysis, Data curation. **Thomas Oommen:** Writing – review & editing, Supervision, Project administration, Methodology, Funding acquisition, Conceptualization. **Pengfei Xue:** Writing – review & editing, Supervision, Project administration, Methodology, Investigation. **Guy Meadows:** Writing – review & editing, Supervision, Project administration. **Navin Tony Thalakkottukara:** Writing – review & editing, Resources, Investigation, Formal analysis. **Ryan Williams:** Writing – review & editing, Resources, Project administration, Data curation.

Declaration of Competing Interest

The authors declare that they have no known competing financial interests or personal relationships that could have appeared to influence the work reported in this paper.

Acknowledgments

The authors acknowledge the financial support from the US National Science Foundation (Award No 2133279) to conduct this research. The analytical capabilities of the RHRT have been extended under the C-CHRAM, a US Department of Energy-funded climate resilience center (DE-SC0024446) at Michigan Technological University. Special thanks to the Western Upper Peninsula Planning Development Region for facilitating data collection and community engagement.

References

Afshari, S., Tavakoly, A.A., Rajib, M.A., Zheng, X., Follum, M.L., Omranian, E., Fekete, B. M., 2018. Comparison of new generation low-complexity flood inundation mapping tools with a hydrodynamic model. J. Hydrol. 556, 539–556. https://doi.org/10.1016/j.jhydrol.2017.11.036.

Andreadis, K.M., Schumann, G.-J.-P., Pavelsky, T., 2013. A simple global river bankfull width and depth database. Water Resour. Res. 49 (10), 7164–7168. https://doi.org/10.1002/wrcr.20440.

Aristizabal, F., Salas, F., Petrochenkov, G., Grout, T., Avant, B., Bates, B., Spies, R., Chadwick, N., Wills, Z., Judge, J., 2023. Extending height above nearest drainage to model multiple fluvial sources in flood inundation mapping applications for the U.S. National Water Model. Water Resour. Res. 59 (5). https://doi.org/10.1029/2022WR032039 e2022WR032039.

Blum, A.G., Ferraro, P.J., Archfield, S.A., Ryberg, K.R., 2020. Causal effect of impervious cover on annual flood magnitude for the United States. Geophys. Res. Lett. 47 (5), e2019GL086480. https://doi.org/10.1029/2019GL086480.

Bornhorst, T. J., and Barron, R. J., 2011. Copper deposits of the western Upper Peninsula of Michigan. In Archean to Anthropocene: Field guides to the geology of the mid-continent of North America (pp. 83–99). Geol. Soc. Am. 10.1130/2011.0024(05).

Chaudhuri, C., Gray, A., Robertson, C., 2021. InundatEd-v1.0: A height above nearest drainage (HAND)-based flood risk modeling system using a discrete global grid system. Geosci. Model Dev. 14 (6), 3295–3315. https://doi.org/10.5194/gmd-14-3295-2021.

Cigler, B.A., 2017. U.S. Floods: The Necessity of Mitigation. State Local Govern. Rev. 49 (2), 127–139. https://doi.org/10.1177/0160323X17731890.

Dewitz, J., 2023. National Land Cover Database (NLCD) 2021 Products. Geological Survey, U.S, 10.5066/P9JZ7AO3.

Di Baldassarre, G., Kooy, M., Kemerink, J.S., Brandimarte, L., 2013. Towards understanding the dynamic behaviour of floodplains as human-water systems. Hydrol. Earth Syst. Sci. 17 (8), 3235–3244. https://doi.org/10.5194/hess-17-3235-2013.

Diehl, R.M., Gourevitch, J.D., Drago, S., Wemple, B.C., 2021. Improving flood hazard datasets using a low-complexity, probabilistic floodplain mapping approach. *PLoS One* 16 (3), e0248683. https://doi.org/10.1371/journal.pone.0248683.

Dreier, N., Männikus, R., and Fröhle, P., 2020. Long-term Changes of Waves at the German Baltic Sea Coast*.* J Coast Res*,* 1416–1421. JSTOR.

EGLE., 2020. National Wetland Inventory (NWI) 2005. Michigan Dept. of Environment, Great Lakes, and Energy Open Data. https://gis-michigan.opendata.arcgis.com/datasets/d6e1bb68c5964731b38d3a7a4a687086_9/about.

Fang, L., Zhang, Z., Huang, J., 2023. Rapid flood modelling using HAND-FFA-SRC coupled approach and social media-based geodata in a coastal Chinese watershed. Environ. Model Softw. 170, 105862. https://doi.org/10.1016/j.envsoft.2023.105862.

Farrand, W.R., Bell, D.L., 1982. Quaternary geology of Northern Michigan [Map]. Michigan Department of Natural Resources, Michigan Geological Survey https://gis-egle.hub.arcgis.com/datasets/egle::quaternary-geology-map/about.

FEMA., 2009. Multi-Hazard Loss Estimation Methodology, Flood Model, HAZUS® MH, Technical Manual. Department of Homeland Security, Federal Emergency Management Agency, Mitigation Division. https://www.fema.gov/flood-maps/tools-resources/flood-map-products/hazus/user-technical-manuals.

FEMA, 2011. Supplement to the benefit-cost analysis—Reference guide. Federal Emergency Management Agency. https://www.fema.gov/sites/default/files/2020-08/fema_bca_guide-supplement.pdf.

FEMA., 2023. National risk index: Technical documentation. https://www.fema.gov/sites/default/files/documents/fema_national-risk-index_technical-documentation.pdf.

First Street Foundation, 2019. FEMA flood maps and limitations. https://medium.com/firststreet/fema-flood-maps-and-limitations-ea06bf103c4d.

Follum, M. L., 2013. AutoRoute rapid flood inundation model (ERDC/CHL CHETN-IV-88; p. 12). US Army Engineer Research and Development Center,Coastal and Hydraulics Laboratory. https://apps.dtic.mil/sti/tr/pdf/ADA583052.pdf.

Früh-Müller, A., Wegmann, M., Koellner, T., 2015. Flood exposure and settlement expansion since pre-industrial times in 1850 until 2011 in north Bavaria, Germany. Reg. Environ. Change 15 (1), 183–193. https://doi.org/10.1007/s10113-014-0633-9.

Garousi-Nejad, I., Tarboton, D.G., Aboutalebi, M., Torres-Rua, A.F., 2019. Terrain analysis enhancements to the height above nearest drainage flood inundation mapping method. Water Resour. Res. 55 (10), 7983–8009. https://doi.org/10.1029/2019WR024837.

Godbout, L., Zheng, J.Y., Dey, S., Eyelade, D., Maidment, D., Passalacqua, P., 2019. Error assessment for height above the nearest drainage inundation mapping. JAWRA Am. Water Resour. Assoc. 55 (4), 952–963. https://doi.org/10.1111/1752-1688.12783.

Grigg, N.S., 2023. comprehensive flood risk assessment: state of the practice. Hydrol 10 (2), 46. https://doi.org/10.3390/hydrology10020046.

Gronewold, A.D., Do, H.X., Mei, Y., Stow, C.A., 2021. A Tug-of-War within the hydrologic cycle of a continental freshwater basin. Geophys. Res. Letters 48 (4), e2020GL090374. https://doi.org/10.1029/2020GL090374.

Gronewold, A.D., Rood, R.B., 2019. Recent water level changes across Earth's largest lake system and implications for future variability. J. Great Lakes Res. 45 (1), 1–3. https://doi.org/10.1016/j.jglr.2018.10.012.

Gutenson, J.L., Tavakoly, A.A., Islam, M.S., Wing, O.E.J., Lehman, W.P., Hamilton, C.O., Wahl, M.D., Massey, T.C., 2023. Comparison of estimated flood exposure and consequences generated by different event-based inland flood inundation maps. Nat. Hazard Earth System Sci. 23 (1), 261–277. https://doi.org/10.5194/nhess-23-261-2023.

Han, Y., Huang, Q., He, C., Fang, Y., Wen, J., Gao, J., Du, S., 2020. The growth mode of built-up land in floodplains and its impacts on flood vulnerability. Sci. Total Environ. 700, 134462. https://doi.org/10.1016/j.scitotenv.2019.134462.

Holtschlag, D. J., and Croskey, H. M., 1984. Statistical models for estimating flow characteristics of Michigan streams (USGS Water-Resources Investigations Report 84–4207).

Hu, A., Demir, I., 2021. Real-time flood mapping on client-side web systems using HAND model. Hydrol 8 (2), 65. https://doi.org/10.3390/hydrology8020065.

Hu, P., Zhang, Q., Shi, P., Chen, B., Fang, J., 2018. Flood-induced mortality across the globe: spatiotemporal pattern and influencing factors. Sci. Total Environ. 643, 171–182. https://doi.org/10.1016/j.scitotenv.2018.06.197.

Huang, C., Zhu, L., Ma, G., Meadows, G.A., Xue, P., 2021. Wave climate associated with changing water level and ice cover in Lake Michigan. Front. Mar. Sci. 8, 746916. https://doi.org/10.3389/fmars.2021.746916.

Huang, H., Fischella, M.R., Liu, Y., Ban, Z., Fayne, J.V., Li, D., Cavanaugh, K.C., Lettenmaier, D.P., 2022. Changes in Mechanisms and Characteristics of Western U.S. Floods Over the Last Sixty Years. Geophys. Res. Letters 49 (3), e2021GL097022. https://doi.org/10.1029/2021GL097022.

Jafarzadegan, K., Merwade, V., 2019. Probabilistic floodplain mapping using HAND-based statistical approach. Geomorphology 324, 48–61. https://doi.org/10.1016/j.geomorph.2018.09.024.

Jafarzadegan, K., Muñoz, D.F., Moftakhari, H., Gutenson, J.L., Savant, G., Moradkhani, H., 2022. Real-time coastal flood hazard assessment using DEM-based hydrogeomorphic classifiers. Nat. Hazard. Earth System Sci. 22 (4), 1419–1435. https://doi.org/10.5194/nhess-22-1419-2022.

Jennings, M. E., Thomas, W. O., Jr., and Riggs, H. C., 1994. Nationwide summary of U.S. Geological Survey regional regression equations for estimating magnitude and frequency of floods for ungaged sites (94–4002; Water-Resources Investigations Report). U.S. Geological Survey. https://pubs.usgs.gov/wri/1994/4002/report.pdf.

Johnson, J.M., Munasinghe, D., Eyelade, D., Cohen, S., 2019. An integrated evaluation of the National Water Model (NWM)–Height Above Nearest Drainage (HAND) flood mapping methodology. Nat Hazard. Earth System Sci. 19 (11), 2405–2420. https://doi.org/10.5194/nhess-19-2405-2019.

Kayastha, M.B., Ye, X., Huang, C., Xue, P., 2022. Future rise of the Great Lakes water levels under climate change. J. Hydrol. 612, 128205. https://doi.org/10.1016/j.jhydrol.2022.128205.

Li, Z., Demir, I., 2022. A comprehensive web-based system for flood inundation map generation and comparative analysis based on height above nearest drainage. Sci. Total Environ. 828, 154420. https://doi.org/10.1016/j.scitotenv.2022.154420.

Li, Z., Demir, I., 2024. MultiRS flood mapper: A google earth engine application for water extent mapping with multimodal remote sensing and quantile-based postprocessing. Environ. Model. Softw. 176, 106022. https://doi.org/10.1016/j.envsoft.2024.106022.

Liu, Y.Y., Maidment, D.R., Tarboton, D.G., Zheng, X., Wang, S., 2018. A CyberGIS integration and computation framework for high-resolution continental-scale flood inundation mapping. JAWRA Am. Water Resour. Assoc. 54 (4), 770–784. https://doi.org/10.1111/1752-1688.12660.

Mase, H., 1989. Random wave runup height on gentle slope. J. Waterw. Port. Coast Ocean Eng. 115 (5), 649–661. https://doi.org/10.1061/(ASCE)0733-950X(1989)115:5(649).

Mazzoleni, M., Mård, J., Rusca, M., Odongo, V., Lindersson, S., Di Baldassarre, G., 2021. Floodplains in the anthropocene: a global analysis of the interplay between human population, built environment, and flood severity. Water Resour. Res. 57 (2), e2020WR027744. https://doi.org/10.1029/2020WR027744.

McDermott, T.K.J., 2022. Global exposure to flood risk and poverty. Nat. Commun. 13 (1), 3529. https://doi.org/10.1038/s41467-022-30725-6.

MRCC., 2012. Historical climatology: Western Upper Michigan. Midwestern Regional Climate Center. https://glisa.umich.edu/media/files/climaticdivs/michigan/Michigan_Climatic_Division_1.pdf.

NOAA, 2022. NOAA Atlas 14 precipitation frequency estimates in GIS compatible format. National Oceanic and Atmospheric Administration, National Weather Service. https://hdsc.nws.noaa.gov/pfds/pfds_gis.html.

Nobre, A.D., Cuartas, L.A., Hodnett, M., Rennó, C.D., Rodrigues, G., Silveira, A., Waterloo, M., Saleska, S., 2011. Height Above the Nearest Drainage – a hydrologically relevant new terrain model. J. Hydrol. 404 (1–2), 13–29. https://doi.org/10.1016/j.jhydrol.2011.03.051.

NWS, 2018. 2018 Father's Day weekend: Upper Michigan flooding. https://www.weather.gov/mqt/fathersday2018weekendflooding.

Rennó, C.D., Nobre, A.D., Cuartas, L.A., Soares, J.V., Hodnett, M.G., Tomasella, J., Waterloo, M.J., 2008. HAND, a new terrain descriptor using SRTM-DEM: Mapping terra-firme rainforest environments in Amazonia. Remote Sens. Environ. 112 (9), 3469–3481. https://doi.org/10.1016/j.rse.2008.03.018.

Rentschler, J., Avner, P., Marconcini, M., Su, R., Strano, E., Vousdoukas, M., Hallegatte, S., 2023. Global evidence of rapid urban growth in flood zones since 1985. Nat 622 (7981), 87–92. https://doi.org/10.1038/s41586-023-06468-9.

Rentschler, J., Salhab, M., Jafino, B.A., 2022. Flood exposure and poverty in 188 countries. Nat. Commun. 13 (1), 3527. https://doi.org/10.1038/s41467-022-30727-4.

Richardson, C.A., Beighley, R.E., 2024. Optimizing Height Above Nearest Drainage parameters to enable rapid flood mapping in North Carolina. Front. Water 5, 1296434. https://doi.org/10.3389/frwa.2023.1296434.

Ries, K. G., III, Steeves, P. A., and McCarthy, P., 2024. StreamStats—A quarter century of delivering web-based geospatial and hydrologic information to the public, and lessons learned (U.S. Geological Survey Circular 1514; Circular, p. 40). 10.3133/cir1514.

Saint-Geours, N., Grelot, F., Bailly, J.-S., Lavergne, C., 2015. Ranking sources of uncertainty in flood damage modelling: A case study on the cost-benefit analysis of a flood mitigation project in the Orb Delta, France. J. Flood Risk Manag. 8 (2), 161–176. https://doi.org/10.1111/jfr3.12068.

Scawthorn, C., Blais, N., Seligson, H., Tate, E., Mifflin, E., Thomas, W., Murphy, J., and Jones, C., 2006a. HAZUS-MH Flood Loss Estimation Methodology. I: Overview and Flood Hazard Characterization. Nat. Hazards Rev, *7*(2), 60–71. 10.1061/(ASCE)1527-6988(2006)7:2(60).

Scawthorn, C., Flores, P., Blais, N., Seligson, H., Tate, E., Chang, S., Mifflin, E., Thomas, W., Murphy, J., Jones, C., and Lawrence, M. 2006b. HAZUS-MH Flood Loss Estimation Methodology. II. Damage and Loss Assessment. Nat Hazards Rev, *7*(2), 72–81. 10.1061/(ASCE)1527-6988(2006)7:2(72).

Schneider, P.J., Schauer, B.A., 2006. HAZUS—Its Development and Its Future. Nat. Hazards Rev. 7 (2), 40–44. https://doi.org/10.1061/(ASCE)1527-6988(2006)7:2(40).

Scriven, B.W.G., McGrath, H., Stefanakis, E., 2021. CERC-HAND-D: A tool for supporting on-the-fly flood mapping in Canada. IEEE Int. Geosci. Remote Sens. Symposium IGARSS 2021, 519–522. https://doi.org/10.1109/IGARSS47720.2021.9553519.

Smith, A. B., 2024. U.S. Billion-dollar Weather and Climate Disasters, 1980—Present (NCEI Accession 0209268). 10.25921/STKW-7W73.

Steinschneider, S., 2021. A hierarchical Bayesian model of storm surge and total water levels across the Great Lakes shoreline – Lake Ontario. J. Great Lakes Res. 47 (3), 829–843. https://doi.org/10.1016/j.jglr.2021.03.007.

Swain, D.L., Wing, O.E.J., Bates, P.D., Done, J.M., Johnson, K.A., Cameron, D.R., 2020. Increased flood exposure due to climate change and population growth in the United States. Earth's Future 8 (11), e2020EF001778. https://doi.org/10.1029/2020EF001778.

Swiss Re., 2023. Natural catastrophes in focus: Floods. https://www.swissre.com/risk-knowledge/mitigating-climate-risk/floods.html.

Tate, E., Muñoz, C., Suchan, J., 2015. Uncertainty and sensitivity analysis of the HAZUS-MH flood model. Nat. Hazards Rev. 16 (3), 04014030. https://doi.org/10.1061/(ASCE)NH.1527-6996.0000167.

Teng, J., Jakeman, A.J., Vaze, J., Croke, B.F.W., Dutta, D., Kim, S., 2017. Flood inundation modelling: a review of methods, recent advances and uncertainty analysis. Environ. Model Softw. 90, 201–216. https://doi.org/10.1016/j.envsoft.2017.01.006.

Thalakkottukara, N.T., Thomas, J., Watkins, M.K., Holland, B.C., Oommen, T., Grover, H., 2024. Suitability of the height above nearest drainage (HAND) model for flood inundation mapping in data-scarce regions: a comparative analysis with hydrodynamic models. Earth Sci Inform. https://doi.org/10.1007/s12145-023-01218-x.

Tripathy, P., Malladi, T., 2022. Global Flood Mapper: A novel Google Earth Engine application for rapid flood mapping using Sentinel-1 SAR. Nat. Hazards 114 (2), 1341–1363. https://doi.org/10.1007/s11069-022-05428-2.

Unnithan, S.L.K., Biswal, B., Rüdiger, C., Dubey, A.K., 2024. A novel conceptual flood inundation model for large scale data-scarce regions. Environ Model Softw. 171, 105863. https://doi.org/10.1016/j.envsoft.2023.105863.

USEPA, 2020. Dasymetric Allocation of Population, Conterminous U.S. (Version 1.1) [Dataset]. EnviroAtlas national data, U.S. Environmental Protection Agency, U.S. Geological Survey, U.S. Department of Agriculture. https://www.epa.gov/enviroatlas/data-download-step-2?token=pZx2iS8j7lS0GZipyG1fhD3moM5EmH8CBWQB1oAI5aY.

Wasko, C., Nathan, R., Stein, L., O'Shea, D., 2021. Evidence of shorter more extreme rainfalls and increased flood variability under climate change. J. Hydrol. 603, 126994. https://doi.org/10.1016/j.jhydrol.2021.1269940.

Wing, O.E.J., Bates, P.D., Smith, A.M., Sampson, C.C., Johnson, K.A., Fargione, J., Morefield, P., 2018. Estimates of present and future flood risk in the conterminous United States. *Environ. Res. Letters* 13 (3), 034023. https://doi.org/10.1088/1748-9326/aaac65.

Winsemius, H.C., Aerts, J.C.J.H., Van Beek, L.P.H., Bierkens, M.F.P., Bouwman, A., Jongman, B., Kwadijk, J.C.J., Ligtvoet, W., Lucas, P.L., van Vuuren, D.P., Ward, P.J., 2016. Global drivers of future river flood risk. Nat. Clim. Chang. 6 (4), 381–385. https://doi.org/10.1038/nclimate2893.

Wu, Q., Lane, C.R., Li, X., Zhao, K., Zhou, Y., Clinton, N., DeVries, B., Golden, H.E., Lang, M.W., 2019. Integrating LiDAR data and multi-temporal aerial imagery to map wetland inundation dynamics using Google Earth Engine. Remote Sens. Environ. 228, 1–13. https://doi.org/10.1016/j.rse.2019.04.015.

WUPPDR, 2020. Houghton county: 2020–2025 hazard mitigation plan (p. 262). Western U.P. Planning and Development Region. https://www.cityofhoughton.com/wp-content/uploads/2020/07/HoughtonCountyHazardMitigationPlan.pdf.

Zheng, X., Maidment, D.R., Tarboton, D.G., Liu, Y.Y., Passalacqua, P., 2018a. GeoFlood: large-scale flood inundation mapping based on high-resolution terrain analysis. Water Resour. Res. 54 (12). https://doi.org/10.1029/2018WR023457.

Zheng, X., Tarboton, D.G., Maidment, D.R., Liu, Y.Y., Passalacqua, P., 2018b. River channel geometry and rating curve estimation using height above the nearest drainage. JAWRA Am. Water Resour. Assoc. 54 (4), 785–806. https://doi.org/10.1111/1752-1688.12661.